Enhancement and suppression of energy transfer from Si nanocrystals to Er ions through a control of the photonic mode density

Nakamura, Toshihiro

Miura, Satoru

Inui, Masaki

Fujii, Minoru

Hayashi, Shinji

Enhancement and suppression of energy transfer from Si nanocrystals to Er ions through a control of the photonic mode density

Toshihiro Nakamura, Minoru Fujii,[*] Satoru Miura, Masaki Inui, and Shinji Hayashi

Department of Electrical and Electronics Engineering, Faculty of Engineering, Kobe University, Rokkodai, Nada,
Kobe 657-8501, Japan

The rate of energy transfer from Si nanocrystals to Er ions was modified by placing a Au layer nearby. The distance between the active layer and the Au layer as well as the wavelength were changed systematically to quantitatively discuss how the energy transfer rate is modified by the photonic mode density. It was found that at particular combinations of the spacer thickness and the wavelength the energy transfer was strongly suppressed, while at other combinations it was enhanced. In order to understand the oscillation behavior of the energy transfer rate, a model fitting was performed. By assuming that the energy transfer rate is proportional to the square of the photonic mode density, the observed oscillation behavior could be well reproduced, and from the fitting the energy transfer rate could be estimated. The estimated rates of energy transfer to the $^4I_{11/2}$ and $^4I_{9/2}$ states of Er^{3+} were about 31 and 5.7 ks^{-1}, respectively.

I. INTRODUCTION

Si nanocrystals (Si-nc's) act as an efficient photosensitizer for Er^{3+} ions.[1–5] The effective absorption cross section of Er^{3+} is strongly enhanced because of large absorption cross section of Si-nc's and efficient energy transfer from Si-nc's to Er ions. Since Si-nc's have a broad absorption band, Er ions placed near Si-nc's can be excited by white light. One of the promising applications of the sensitization effect is a compact planar type optical amplifier operating at the 1.54 μm range.[6]

In a previous work,[7] we demonstrated that the rate of energy transfer is modified by placing a Au layer near a SiO$_2$ film containing Si-nc's and Er. The rate oscillates with increasing the separation between the active layer and a Au layer. The oscillation period coincides with that of the calculated photonic mode density (PMD), suggesting that the energy transfer rate can be modified by changing the PMD. However, quantitative analysis of the oscillation behavior could not be made in the previous work. In particular, the amplitude of the oscillation, which was much larger than that expected from the calculated PMD, was not explained even qualitatively. Furthermore, the energy dependence of the oscillation behavior was not studied in detail. Since there are several discrete energy transfer channels between Si-nc's and Er^{3+}, the information about the energy dependence of the energy transfer rate and that of the oscillation behavior is indispensable to fully understand how the process is modified by the PMD.

This work is an extension of the previous work. In this work, we study the effect of a Au thin layer on the energy transfer rate from Si-nc's to Er ions in a wide wavelength range. We show that the energy transfer rate depends strongly on the wavelength and the distance between Si-nc's and the Au layer. In order to quantitatively explain the dependence totally, we constructed a model which assumes that the energy transfer rate is proportional to the square of the PMD, and tried to fit the model to the experimental data. We demonstrate that the model can reproduce the experimentally

obtained oscillation behavior quite well in the whole wavelength range, and from the fitting the energy transfer rate can be estimated as a function of the wavelength. We show that the energy transfer rate increases abruptly above the energy of the $^4I_{9/2}$ state of Er^{3+}. We also show that by Er doping nonradiative recombination rate of Si-nc's is strongly suppressed.

II. EXPERIMENTAL PROCEDURE

The samples studied consist of four layers as schematically shown in the inset of Fig. 1. First, SiO$_2$ films containing Si-nc's (Si-nc:SiO$_2$) or Si-nc's and Er (Si-nc:Er:SiO$_2$) with a thickness of about 150 nm were deposited by the cosputtering of Si and SiO$_2$ (and Er$_2$O$_3$) on a SiO$_2$ substrate.[8] The films were then annealed in a nitrogen gas atmosphere for 30 min at 1200 °C to grow Si-nc's and to activate Er ions. In this process, the size of the Si-nc's can be controlled by changing the excess Si concentration or the annealing temperature. The Er concentration was fixed to 0.11 at. %. After the growth of the Si-nc's, a SiO$_2$ spacer layer was sputter deposited on the active layer. During the sputtering, a mask was continuously translated and the thickness of the spacer layer was changed continuously from 0 to 540 nm. Finally, a Au thin layer (about 100 nm in thickness) was deposited by vacuum evaporation.

The excitation source for photoluminescence (PL) measurements was 457.9 nm light from an optical parametric oscillator pumped by the third harmonic of a neodymium-doped yttrium aluminum garnet (Nd:YAG) laser (pulse energy 0.5 mJ/cm^2, pulse width 5 ns, and repetition frequency 20 Hz). The excitation and the detection of PL were made through a transparent fused quartz substrate. The PL spectra were recorded by using a single-grating monochromator equipped with a liquid-nitrogen-cooled InGaAs near-infrared diode array. For the time response measurements, the luminescence signal was detected by a near-infrared photomultiplier (R5509-72, Hamamatsu) and the decay curves were recorded by a multichannel scalar (SR430, Stanford Research).
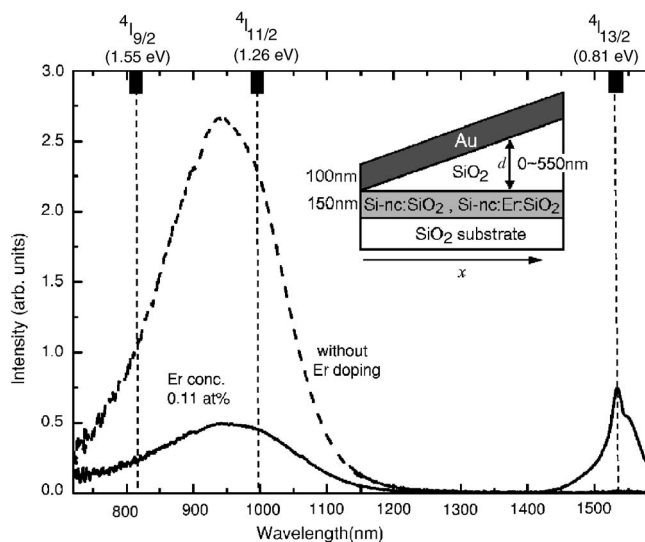
FIG. 1. PL spectra of a SiO_2 film containing Si-nc's and one containing Si-nc's and Er (0.11 at. %). The broad emission band at around 1.27 eV is due to the recombination of excitons in Si-nc and the sharp peak at 0.81 eV arises from the intra-4f-shell transition of Er^{3+} ($^4I_{13/2} \rightarrow {}^4I_{15/2}$). Inset: schematic representation of the sample structure. SiO_2 active layer containing Si-nc's (Si-nc:SiO_2) or Si-nc's and Er (Si-nc:Er:SiO_2) is deposited on a SiO_2 substrate. On the active layer a SiO_2 spacer layer and a Au thin layer (100 nm) are deposited.

The overall time resolution of the system was better than 100 ns. To obtain the spacer thickness dependence of the PL decay curves, samples were mounted on a computer-controlled linear stage and the decay curves were measured by changing the position in the x direction (see the inset of Fig. 1). The variation of the spacer thickness (Δd) in each measurement is smaller than 20 nm. At each position the decay curves were recorded in the wavelength range from 760 to 1040 nm with a step of 20 nm. All measurements were performed at room temperature.

III. RESULTS

A. Wavelength dependence of energy transfer rate

Before studying the effect of a Au layer on the rate of energy transfer from Si-nc's to Er ions, we clarify the wavelength dependence of the rate for samples without a Au layer. Figure 1 shows PL spectra of Si-nc:SiO_2 and Si-nc:Er:SiO_2 samples. A broad emission band around 980 nm is due to the recombination of excitons in Si-nc's and the sharp one at 1530 nm to the intra-4f-shell transition of Er^{3+}. By Er doping, PL from Si-nc's is quenched. The quenching is caused by the energy transfer from Si-nc's to Er ions. In the inset of Fig. 2, the decay rates of PL from Si-nc's are plotted as a function of the emission wavelength for samples with (closed squares) and without (open squares) Er doping. The decay rates are obtained by fitting the PL decay curves with a stretched exponential function. The increase in the decay rate in the shorter-wavelength region is caused by a larger overlap of electron and hole wave functions in a
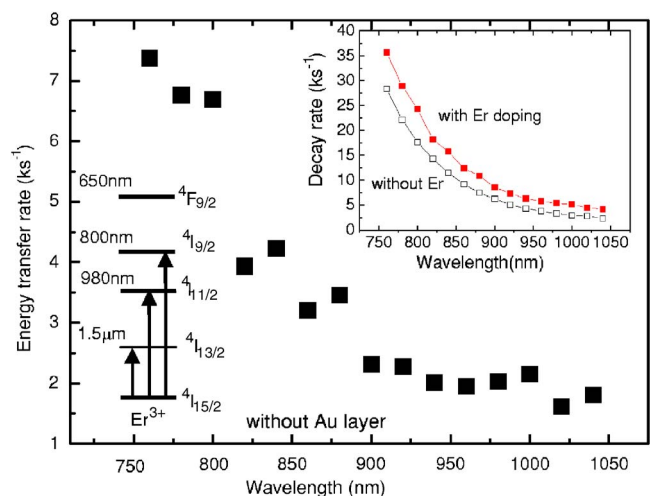

FIG. 2. (Color online) Energy transfer rate from Si nanocrystals to Er ions as a function of the wavelength for the sample without a Au layer. Inset: PL decay rates of Si nanocrystals for the samples with (closed squares) and without (open squares) Er doping.

momentum space by the quantum confinement effect.[9] On Er doping, the rate is increased in the whole wavelength range. The increase in the rate is evidence of the nonradiative energy transfer from Si-nc's to Er ions.

If the increase in the decay rate by Er doping is caused only by the energy transfer, the rate of the energy transfer can be estimated by subtracting the PL decay rate of Si-nc's without Er from that with Er. Figure 2 shows the energy transfer rate estimated by this procedure as a function of the wavelength. In Fig. 2, we see that the energy transfer rate is larger at shorter wavelengths. It is worth noting that the energy transfer rate is not a smooth function of the wavelength, and steps can be seen at around 1000 and 800 nm, although the data are slightly scattered. These wavelengths correspond to the excitation of Er^{3+} to the $^4I_{11/2}$ and $^4I_{9/2}$ states (see energy level diagram of Er^{3+} in the inset of Fig. 2).

B. Energy transfer from Si nanocrystals to Er ions on a Au layer

In previous work,[7] we showed that the decay rate of PL from Si-nc's at 1.26 eV ($\sim$980 nm) oscillates depending on the separation between the active layer and the Au layer. The oscillation results from the destructive or constructive interference of the emitter field with the reflected one, and the energy transfer from Si-nc's to surface plasmon modes and lossy wave modes in the metal.[7,10,11] We also showed that the amplitude of the oscillation obtained for Si-nc:Er:SiO_2 is much larger than that for Si-nc:SiO_2, while the periods of the oscillation are the same. In this work, we study the wavelength dependence of the oscillation behavior. Figures 3(a) and 3(b) show some of the results. The detection wavelengths are 780, 820, 860, 900, 940, 980, and 1020 nm. Closed and open symbols represent the decay rates for the samples with and without Er doping, respectively. Note that the scale of the vertical axis is different between Figs. 3(a) and 3(b). We can see that the amplitude of the oscillation is
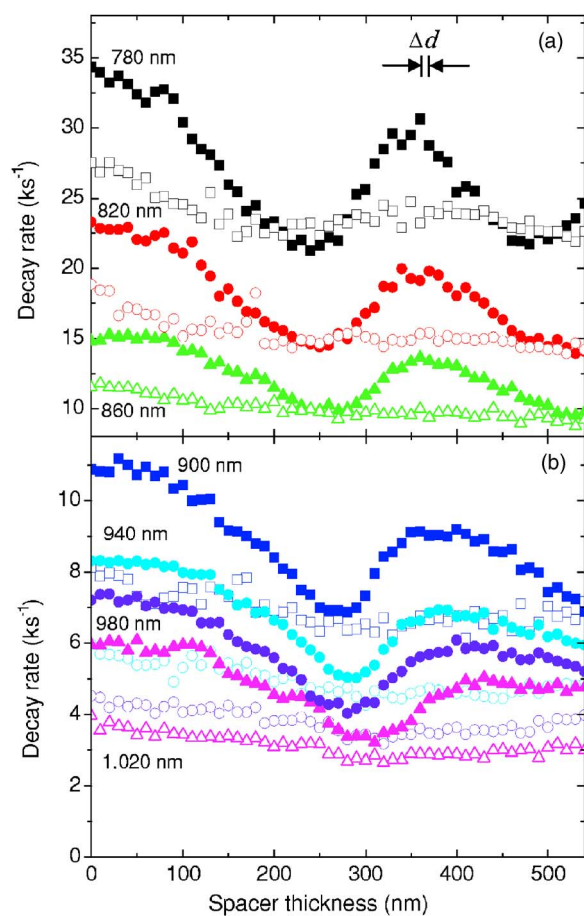
FIG. 3. (Color online) Decay rates of Si nanocrystals for the samples with a Au layer on top as a function of spacer thickness. The spacer thicknesses are changed from 0 to 540 nm. Closed and open squares represent the decay rates for the samples with and without Er doping, respectively. Detection wavelengths are (a) 780, 840, and 880 nm, (b) 900, 940, 980, and 1020 nm from the top to the bottom. Note that the scale of the vertical axis is different between (a) and (b).

strongly enhanced by Er doping in the whole wavelength range. The strong enhancement of the oscillation amplitude implies that the rate of the energy transfer from Si-nc's to Er ions is modified by the presence of the Au layer. In Fig. 3, we also see that with increasing wavelength the period of the oscillation becomes longer and the second peak of the oscillation shifts to larger spacer thickness. It is very interesting to note that the enhancement of the decay rate by Er doping is almost suppressed, i.e., the decay rates of the sample with and without Er doping are almost the same at spacer thicknesses around 270 and 500 nm. These behaviors are qualitatively the same as those shown in the previous paper.[7] However, there are quantitative differences. For example, for the sample without Er doping the oscillation amplitude at a small spacer thickness region in the present data is slightly smaller than that in the previous data. This difference is considered to arise from inaccuracy of the spacer thickness control in a small thickness range in the previous work.

By applying the procedure mentioned above we estimate the energy transfer rate as a function of spacer thickness and
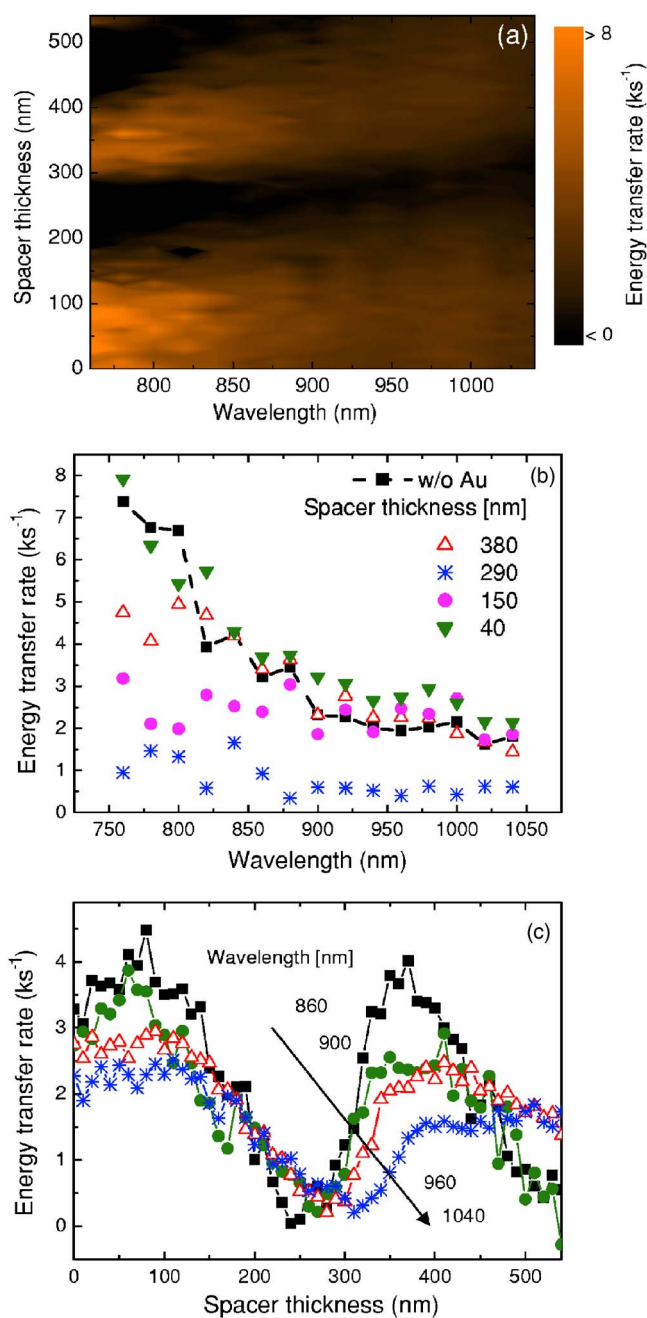

FIG. 4. (Color online) (a) Energy transfer rates as functions of spacer thickness (left axis) and detection wavelength (bottom axis). The color scale is chosen such that the dark regions represent the small energy transfer rate. (b) Energy transfer rates as a function of the wavelength for various spacer thicknesses (40, 150, 290, and 380 nm). The rate for the sample without a Au layer is also shown (closed squares with broken lines). (c) Spacer thickness dependence of the energy transfer rate. The detection wavelengths are 860, 900, 960, and 1040 nm.

of detection wavelength. The gray-scale map in Fig. 4(a) shows the energy transfer rate as a function of the spacer thickness (left axis) and of the wavelength (bottom axis). The gray scale is chosen such that the dark regions represent the small energy transfer rate. We see that the energy transfer rate depends on both the spacer thickness and the emission

wavelength. In Figs. 4(b) and 4(c), energy transfer rates as a function of wavelength for various spacer thicknesses (40, 150, 290, and 380 nm) and spacer thickness dependence of the energy transfer rate at the wavelengths of 860, 900, 960, and 1040 nm are shown. In Fig. 4(b), we can see that the wavelength dependence of the energy transfer rate is significantly different at different spacer thickness. In the figure, for comparison purposes the energy transfer rates for the sample without a Au layer are shown by the square symbols with the broken curve. When the spacer thickness is 40 nm, the energy transfer rate is slightly enhanced in the long-wavelength range, while when the spacer thickness is 290 nm, it is strongly suppressed in the whole wavelength range. In Fig. 4(c), suppression of the energy transfer rate at particular spacer thickness ranges can clearly be seen.

IV. DISCUSSION

The observed oscillation of the decay rate of PL from Si-nc's for the Si-nc:SiO$_2$ sample is explained by the modification of the photonic mode density by the presence of the Au layer.[7] The variation of the decay rate due to the existence of the interface can be calculated using the model developed by Chance *et al.*[10] If the quantum efficiencies of Si-nc's are 100%, the experimentally obtained spacer thickness dependence of the decay rate should be proportional to that of the calculated decay rate, i.e., $W_{\mathrm{expt}}(\lambda,d) = W_{\mathrm{r}}(\lambda)\Gamma(\lambda,d)$, where $W_{\mathrm{expt}}(\lambda,d)$ is the experimentally obtained decay rate at wavelength λ, $W_{\mathrm{r}}(\lambda)$ is the intrinsic radiative decay rate, and $\Gamma(\lambda,d)$ is the spacer thickness dependence of the calculated decay rates normalized to the intrinsic decay rate.

If there are nonradiative decay channels, the above relation does not hold. Under the assumption that the nonradiative rate does not depend on the PMD, the decay rate $W_{\mathrm{expt}}(\lambda,d)$ obtained experimentally is expressed as[12–15]

$$W_{\mathrm{expt}}(\lambda,d) = W_{\mathrm{r}}(\lambda)\Gamma(\lambda,d) + W_{\mathrm{nr}}(\lambda), \quad (1)$$

where $W_{\mathrm{nr}}(\lambda)$ is the nonradiative decay rate of the emitter. By fitting Eq. (1) to the experimentally obtained decay rate vs spacer thickness relation, $W_{\mathrm{r}}(\lambda)$ and $W_{\mathrm{nr}}(\lambda)$ can be obtained.

In the inset of Fig. 5, an example of the result of the fitting is shown. We can see that Eq. (1) can reproduce the oscillation behavior of the experimentally obtained decay rates quite well. The estimated values of $W_{\mathrm{r}}(\lambda)$ and $W_{\mathrm{nr}}(\lambda)$ are plotted as a function of the detection wavelength in Fig. 5. The radiative rate as well as the nonradiative rate increases with decreasing the size of Si-nc's. Although not shown here the radiative rate estimated from this procedure is almost independent of the preparation condition and is on a single universal curve for different samples.[16] On the other hand, the value of the nonradiative rate depends strongly on the preparation process.[16]

As shown in Fig. 3, in the Si-nc:Er:SiO$_2$ sample, the oscillation amplitude of the decay rate is strongly enhanced.
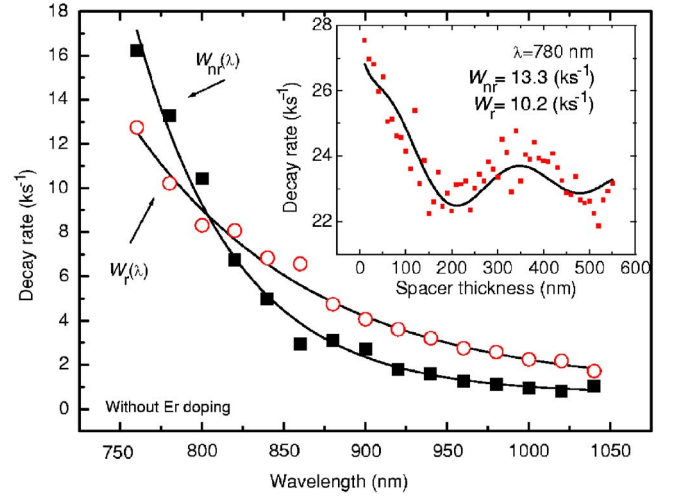

FIG. 5. (Color online) Radiative rate $W_{\mathrm{r}}(\lambda)$ (open circles) and nonradiative rate $W_{\mathrm{nr}}(\lambda)$ (closed squares) of Si nanocrystals for the sample without Er doping as a function of the wavelength. Inset: decay rate of Si nanocrystals detected at 780 nm as a function of spacer thickness (close squares). Solid curve represents the result of the calculation obtained by Eq. (1).

The amplitude is larger than that expected for pure Si-nc's with the quantum efficiency of 100%, and thus the data cannot be fitted by Eq. (1), i.e., W_{nr} becomes negative. This fact suggests that the energy transfer rate is strongly modified by the presence of the Au layer. If we assume that the energy transfer is made by a Förster-type process, the energy transfer rate is proportional to the radiative rate of the energy donor and also that of energy acceptor.[17,18] Since the radiative rate is considered to be linearly dependent on the photonic mode density, the energy transfer rate is expected to be proportional to the square of the photonic mode density. Therefore, the total decay rate of the energy donor is expressed as

$$W_{\mathrm{expt}}(\lambda,d) = W_{\mathrm{r}}(\lambda)\Gamma(\lambda,d) + W_{\mathrm{nr}}^{*}(\lambda) + W_{\mathrm{et}}(\lambda)\Gamma_{\mathrm{r}}^{2}(\lambda,d), \quad (2)$$

where $W_{\mathrm{nr}}^{*}(\lambda)$, $W_{\mathrm{et}}(\lambda)$, and $\Gamma_{\mathrm{r}}(\lambda,d)$ are the nonradiative rate for the Si-nc:Er:SiO$_2$ sample, the energy transfer rate, and the normalized radiative rate obtained by calculation,[7,10] respectively.

In order to verify the validity of this model, we try to fit Eq. (2) to the experimentally obtained decay rates of Si-nc's PL for the Si-nc:Er:SiO$_2$ sample. For the fitting, $W_{\mathrm{r}}(\lambda)$ is not treated as a fitting parameter, but the value obtained in Fig. 5 for the Si-nc:SiO$_2$ sample is used because $W_{\mathrm{r}}(\lambda)$ is insensitive to the local environments of the Si-nc's,[16] i.e., it is considered to be independent of whether Er stays nearby or not. On the other hand, the nonradiative process is very sensitive to the local environment, and thus we cannot adopt the values obtained for the Si-nc:SiO$_2$ sample. Therefore, in Eq. (2), $W_{\mathrm{nr}}^{*}(\lambda)$ and $W_{\mathrm{et}}(\lambda)$ are treated as fitting parameters. The solid curves in the inset of Fig. 6(a) show the results of the fitting at different wavelengths. In all the wavelengths, the agreement between experiment and calculation is quite good except for a very small spacer thickness range. The
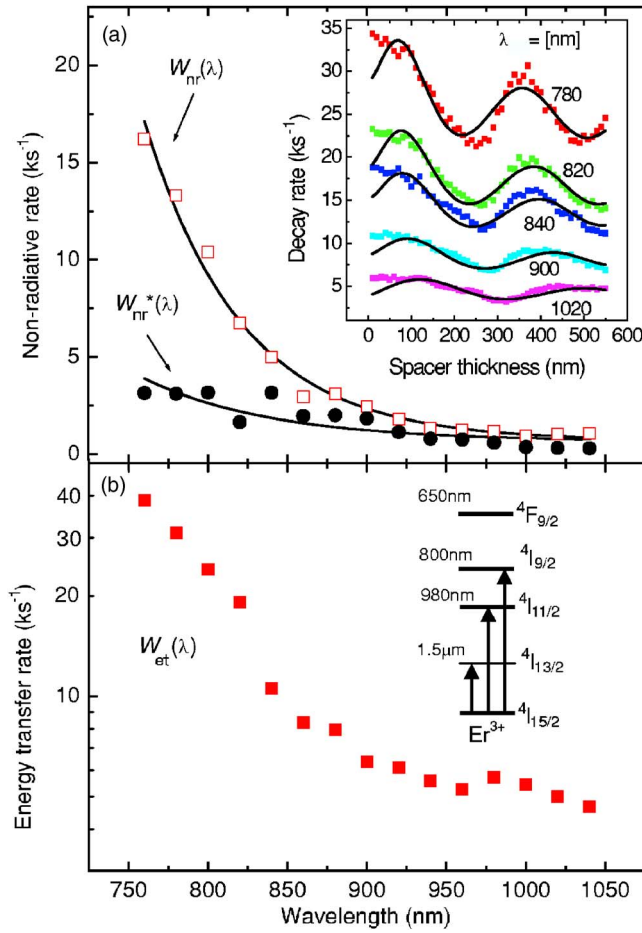
FIG. 6. (Color online) (a) The wavelength dependence of non-radiative rates for the sample with, $W_{nr}^*(\lambda)$ (closed circles) and without, $W_{nr}(\lambda)$ (open squares), Er doping. Inset: decay rates of Si nanocrystals for the sample with Er doping as a function of spacer thickness (close squares). Solid curves are obtained by fitting the data with Eq. (2). (b) The wavelength dependence of energy transfer rate $W_{et}(\lambda)$ (closed squares).

overall agreement implies that the model is in principle correct.

In Fig. 6(a), $W_{nr}(\lambda)$ obtained for the Si-nc:SiO$_2$ sample by using Eq. (1) and $W_{nr}^*(\lambda)$ obtained for the Si-nc:Er:SiO$_2$ sample by applying Eq. (2) are compared. We can see that the nonradiative rates for the sample with Er doping are smaller than those without Er doping in the whole wavelength range. This result implies that nonradiative recombination channels in Si-nc's are reduced by Er doping. In Er-doped amorphous Si thin films, reduction of the number of dangling bonds by Er doping is reported and explained by an exchangelike interaction between the spin of Er^{3+} and that of silicon dangling bonds.[19] A similar mechanism may work in the present system, although not proved in the present work.

In Fig. 6(b), the energy transfer rate W_{et} obtained by fitting is plotted as a function of the wavelength. The energy transfer rate increases as the wavelength shortens. However, in contrast to the radiative and nonradiative rates, the energy transfer rate is not a smooth function of the wavelength. We

can see a small rise of the rate at around 980 nm and a large step around 825 nm. When the band gap energy of a Si-nc is far below the energy of the $^4I_{11/2}$ state of Er^{3+} (980 nm), energy transfer from the Si-nc to the Er ions can be made only to the $^4I_{13/2}$ state by emitting phonons to satisfy the energy conservation rule. If the band gap energy is increased to the energy of the $^4I_{11/2}$ state by decreasing the size, an additional energy transfer channel to the $^4I_{11/2}$ state opens. This results in a rise of the energy transfer rate at around 980 nm as can be seen in Fig. 6(b). Further decrease of the size results in a small decrease of the rate because the band gap energy starts to be away from the resonant energy. Below 950 nm, the rate again starts to increase slightly. The slight increase of the rate is considered to be due to the enhancement of the radiative rate of Si-nc's, i.e., the disadvantage caused by smaller spectral overlap between donors and acceptors is overcome by the advantage due to larger oscillator strength of the energy donor. If the band gap energy approaches the energy of the $^4I_{9/2}$ state, an additional energy transfer channel to the $^4I_{9/2}$ state opens. This results in a steep rise of the rate around 825 nm. The continuous rise of the rate above the energy of $^4I_{9/2}$ state is again considered to be due to the steep rise of the radiative rate of Si-nc's in this range (see Fig. 5).

Figure 6 clearly demonstrates that the energy transfer rate is significantly different between Si-nc's coupled only to the $^4I_{11/2}$ state and those able to couple to the $^4I_{9/2}$ state; the energy transfer rate at the $^4I_{11/2}$ state energy is 5.7 ks^{-1}, while that at the $^4I_{9/2}$ state energy is 31 ks^{-1}. The significant difference means that to achieve efficient energy transfer from Si-nc's to Er ions, the size of the Si-nc's should be small enough to couple to the $^4I_{9/2}$ state, i.e., the band gap energy should be larger than 1.55 eV.

It should be noted that the values of the energy transfer rates in Fig. 6(b) estimated by using Eq. (2) is larger than those obtained by a simple procedure shown in Fig. 2. With a simple procedure, i.e., the subtraction of the PL decay rate of the sample without Er doping (Si-nc:SiO$_2$) from that with Er doping (Si-nc:Er:SiO$_2$), the information about Si-nc's that do not interact with Er^{3+} in samples is included. This leads to an underestimation of the rate. On the other hand, in the procedure in Eq. (2), only the information about Si-nc's interacting with Er^{3+} can be extracted. Therefore, the energy transfer rates shown in Fig. 6(b) are more realistic values.

V. CONCLUSION

The energy transfer rate from Si-nc's to Er ions was modified by placing a Au layer nearby. Clear oscillation of the rate was observed when the separation between the active layer and the Au film was changed from 0 to 540 nm. To quantitatively analyze the oscillation behavior and extract important parameters, a model was proposed. In the model the energy transfer rate is assumed to be proportional to the square of the PMD. The experimental results could be well reproduced by the model. By the fitting, the energy transfer rates were obtained. For large Si-nc's which can couple only to the $^4I_{11/2}$ state of Er^{3+}, the rate was about 5.7 ks^{-1}. On the other hand, for smaller Si-nc's which can couple to the $^4I_{9/2}$

state, the rate was found to be larger than 30 ks^{-1}. The result implies that to achieve efficient energy transfer from Si-nc's to Er ions, the band gap energy of Si-nc's should be larger than the energy of the $^4I_{9/2}$ state. Although the wavelength range studied in this work is limited to 750 nm, it is very interesting to study the energy transfer rate of smaller Si-nc's having band gap energies in the visible range. In these Si-nc's, the energy transfer rate is expected to be much larger because of possible coupling to higher excited states of

Er ions and larger radiative recombination rates of energy donors.

*Author to whom correspondence should be addressed. Electronic address: fujii@eedept.kobe-u.ac.jp

[1] A. J. Kenyon, P. F. Trwoga, M. Federighi, and C. W. Pitt, J. Phys.: Condens. Matter **6**, L319 (1994).

[2] F. Priolo, G. Franzó, D. Pacifici, V. Vinciguerra, F. Iacona, and A. Irrera, J. Appl. Phys. **89**, 264 (2001).

[3] P. G. Kik and A. Polman, J. Appl. Phys. **88**, 1992 (2000).

[4] M. Wojdak, M. Klik, M. Forcales, O. B. Gusev, T. Gregorkiewicz, D. Pacifici, G. Franzó, F. Priolo, and F. Iacona, Phys. Rev. B **69**, 233315 (2004).

[5] J. H. Shin, S. Seo, S. Kim, and S. G. Bishop, Appl. Phys. Lett. **76**, 1999 (2000).

[6] H. Han, S. Seo, and J. Shin, Appl. Phys. Lett. **79**, 4568 (2001).

[7] T. Nakamura, M. Fujii, K. Imakita, and S. Hayashi, Phys. Rev. B **72**, 235412 (2005).

[8] M. Fujii, M. Yoshida, S. Hayashi, and K. Yamamoto, J. Appl. Phys. **84**, 4525 (1998).

[9] T. Takagahara and K. Takeda, Phys. Rev. B **46**, 15578 (1992).

[10] R. R. Chance, A. Prock, and R. Silbey, Adv. Chem. Phys. **37**, 1 (1978).

[11] W. L. Barnes, J. Mod. Opt. **45**, 661 (1998).

[12] R. J. Walters, J. Kalkman, A. Polman, H. A. Atwater, and M. J. A. de Dood, Phys. Rev. B **73**, 132302 (2006).

[13] J. Kalkman, H. Gersen, L. Kuipers, and A. Polman, Phys. Rev. B **73**, 075317 (2006).

[14] E. Snoeks, A. Lagendijk, and A. Polman, Phys. Rev. Lett. **74**, 2459 (1995).

[15] M. J. A. de Dood, L. H. Slooff, A. Polman, A. Moroz, and A. van Blaaderen, Phys. Rev. A **64**, 033807 (2001).

[16] S. Miura, T. Nakamura, M. Fujii, M. Inui, and S. Hayashi, Phys. Rev. B **73**, 245333 (2006).

[17] T. Förster, *Fluorenzenz Organische Verbindungen* (Vandenhoech and Ruprech, Gottingen, 1951).

[18] N. J. Turro, *Modern Molecular Photochemistry* (University Science Books, Sausalito, CA, 1991).

[19] M. S. Sercheli, C. Rettori, and A. R. Zanatta, Phys. Rev. B **68**, 174418 (2005).